Generalized Wavelet Shrinkage of Inline Raman Spectroscopy for Quality Monitoring of Continuous Manufacturing of Carbon Nanotube Buckypaper

Xiaowei Yue, *Member, IEEE*, Kan Wang, Hao Yan, Jin Gyu Park, Zhiyong Liang, Chuck Zhang, Ben Wang, and Jianjun Shi

***Abstract*— Process monitoring and quality control is essential for continuous manufacturing processes of carbon nanotube (CNT) thin sheets or buckypaper. Raman spectroscopy is an attractive inline quality characterization and quantification tool for nanomanufacturing because of its nondestructive nature, fast data acquisition speed, and ability to provide detailed material information. However, there is signal-dependent noise buried in the Raman spectra, which reduces the signal-to-noise (S/N) ratio and affects the accuracy, efficiency, and sensitivity for Raman spectrum-based quality control approaches. In this paper, a signal analysis model with signal-dependent noise for Raman spectroscopy is developed and validated based on experimental data. The wavelet shrinkage method is used for denoising and improving the S/N ratio of raw Raman spectra. Based on the validated signal-noise relationship, a novel generalized wavelet shrinkage approach is introduced to remove noise in all wavelet coefficients by applying individual adaptive wavelet thresholds. The effectiveness of this method is demonstrated using both simulation and experimental case studies of inline Raman monitoring of continuous buckypaper manufacturing. The proposed method allows for a significant reduction of Raman data acquisition time without much loss of S/N ratio, which inherently enables Raman spectroscopy for inline monitoring and control for continuous nanomanufacturing processes.**

***Note to Practitioners*—This paper was motivated by the problem of implementing denoising and signal enhancement for Raman spectra to realize inline process monitoring and quality control of continuous nanomanufacturing of carbon nanotube (CNT) buckypaper. Existing approaches like wavelet denoising cannot deal with signal dependent noise buried in the Raman spectra effectively. This paper develops a signal analysis model and validates the signal-noise dependence property. Then a novel generalized wavelet shrinkage approach is used to remove noise in each wavelet coefficient by applying individual adaptive wavelet threshold. With this new approach, signal-noise ratio can be improved efficiently, and process monitoring accuracy and sensitivity can be enhanced effectively. This paper provides a solid foundation for inline process monitoring and quality control for continuous nanomanufacturing of CNT buckypaper. Furthermore, the developed methodology can be applied into denoising signal-dependent noise in other kinds of signals. In future work, we will develop a process monitoring approach of multistage nanomanufacturing process.**

***Index Terms*— Carbon nanotube (CNT), nanomanufacturing, Raman spectroscopy, signal-dependent noise, wavelet.**

I. Introduction

CARBON NANOTUBE (CNT) buckypaper is an important multifunctional platform material as it has great potential for creating lightweight high-performance materials for various applications. To attain their intrinsic multifunctional properties at the macroscale and scale-up production in continuous forms, CNTs must be effectively and efficiently aligned and covalently interconnected into the desired architecture on the nanoscale. An effective approach for achieving such goals is to make thin (5–25 μm) CNT sheets or "buckypaper" for use as reinforcement or functional layers that have high nanotube loading, good distribution/dispersion, high alignment, and desired intertube connections. The buckypaper has superior mechanical and electrical conductivity performance for applications such as conductive composites and lightweight electricity cable covers for electromagnetic interference shielding. One of the critical roadblocks to scale-up production of high-quality buckypaper is the monitoring and control of buckypaper made from the continuous nanomanufacturing process. As an effective offline characterization method for nanostructure information, Raman spectroscopy has been widely used in batch-to-batch nanomanufacturing of CNT buckypaper materials [1]–[4]. Recently, inline Raman spectroscopy has been developed to monitor biochemical reactions and pharmaceutical crystallizations [5]–[7]. In these

Manuscript received November 20, 2015; revised March 28, 2016; accepted August 5, 2016. Date of publication August 30, 2016; date of current version January 4, 2017. This paper was recommended for publication by Associate Editor Q. Huang and Editor Y. Sun upon evaluation of the reviewers' comments. This work was supported by the NSF Scalable Nanomanufacturing Program under Grant SNM 1344672. *(Corresponding author: Jianjun Shi.)*

X. Yue, K. Wang, H. Yan, and C. Zhang are with the H. Milton Stewart School of Industrial and Systems Engineering, Georgia Institute of Technology, Atlanta, GA 30332 USA (e-mail: xwy@gatech.edu; kwang34@mail.gatech.edu; yanhao@gatech.edu; chuck.zhang@gatech.edu).

J. G. Park and Z. Liang are with the High-Performance Materials Institute, Florida State University, Tallahassee, FL 32310 USA (e-mail: jgpark@fsu.edu; zliang@fsu.edu).

B. Wang is with the H. Milton Stewart School of Industrial and Systems Engineering and the School of Materials Science and Engineering, Georgia Institute of Technology, Atlanta, GA 30332 USA (e-mail: ben.wang@gatech.edu).

J. Shi is with the H. Milton Stewart School of Industrial and Systems Engineering and the George W. Woodruff School of Mechanical Engineering, Georgia Institute of Technology, Atlanta, GA 30332 USA (e-mail: jianjun.shi@isye.gatech.edu).

This paper has supplementary downloadable multimedia material available at http://ieeexplore.ieee.org provided by the authors. The Supplementary Material contains Raman spectra dataset. This material is 871.9 KB in size.

Color versions of one or more of the figures in this paper are available online at http://ieeexplore.ieee.org.

Digital Object Identifier 10.1109/TASE.2016.2599023

efforts, inline Raman spectra were found effective in providing detailed chemical molecular information and nondestructive testing and were accomplished within seconds during continuous reactions or manufacturing processes. For similar purposes, we focus on developing an inline Raman spectroscopy approach that is studied for continuous nanomanufacturing processes for inline quality monitoring and control of continuous nanomanufacturing process and buckypaper materials.

One of the major quality control challenges of using inline Raman spectroscopy is the tradeoff between data acquisition time and signal quality, i.e., signal-to-noise (S/N) ratio due to the samples moving fast compared with regular static tests. A typical Raman characterization takes multiple scans with at least 10 s of acquisition time per scan. The procedure ensures a high S/N ratio, but takes 10 s to several minutes to acquire one spectrum [8], [9]. For inline quality control of the nanomanufacturing process, a shorter data acquisition time with adequate S/N ratio is more desirable because of the following: 1) a shorter data acquisition time will decrease the control bandwidth for process monitoring and control, which will correspondingly enhance the effectiveness and accuracy of quality monitoring and decrease losses from out-of-control situations and 2) it will decrease the material heterogeneity-dependent noise and provide a better inline monitoring capability, as the materials to be inspected are moving quickly in a continuous buckypaper nanomanufacturing process. This would enhance the signal difference from different locations during a continuous test.

A low S/N ratio in a Raman spectrum may create several issues in feature extractions. If the magnitude of noise is comparable with the small peaks caused by impurities or defects in buckypaper, important features could be overlooked. Even if the peaks are distinguishable, a small S/N ratio may cause large uncertainties in the determination of peak positions, peak intensity, and peak width, which causes inaccuracy in the peak analysis. For example, in Raman spectroscopy analysis for CNT buckypaper, the intensity ratio of two peaks is the feature of interest, known as the intensity ratio of D-band and G-band. This ratio can be affected by the degree of functionalization. The intensity ratio of polarized Raman spectrum along the parallel and perpendicular directions to the alignment direction of CNTs in a buckypaper can be used to determine its degree of alignment [10]. In those cases, a low S/N ratio in the Raman spectrum data can be especially problematic since errors in the estimation of uncertainties of peak intensity may have a significant impact on the intensity ratio. Fig. 1 shows the comparison between the Raman spectrum data taken from the same single-walled CNT (SWCNT) buckypaper sample with one pass of different acquisition times. The D-band and G-band are marked in Fig. 1. Also, it is obvious that Raman spectrum with 5-s acquisition time has a higher S/N ratio than the one with 0.5-s acquisition time. This is because that Raman intensity tends to be larger as the increase in the acquisition time, and the effect from a random noise tends to be smaller. Detailed explanations can be found in Sections II-A and II-B.

If the characteristics of the noise are known, it is possible to design a specific filtering technique to take advantage

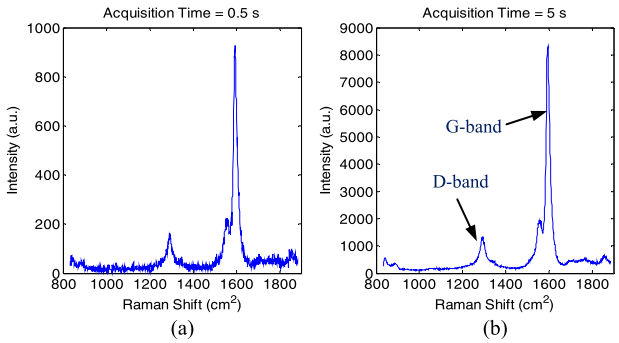

Fig. 1. Typical Raman spectrum data of SWCNT buckypaper with data acquisition time of (a) 0.5 and (b) 5 s, respectively.

of these characteristics and improve the S/N ratio through denoising. Typical denoising methods for nonlinear signals such as Raman spectra include spline and wavelet approaches. The spline basis is smooth, continuously differentiable, and, therefore, has excellent approximation properties for smoothing signals [11]. However, Raman spectrum is not smooth in general and many peaks can exist in the signal, as shown in Fig. 1. Wavelet analysis is one of the most powerful and widely applied tools in time-frequency transformations and denoising because of three advantages: 1) it is an effective nonparametric approach to characterize nonlinear profiles: 2) it effectively extracts time-frequency features in multiple resolutions, which overcomes the limitations of conventional Fourier transform (FT) and short-time FT methods; and 3) the obtained wavelet coefficients are sparse so that signals can be effectively denoised or compressed. Wavelet analysis has been widely used for spike removal, denoising, and signal compression for Raman spectra [12], [13]. Conventional wavelet denoising methods (e.g., VisuShrink, RiskShrink, and SureShrink methods) assume that noise in the signal model is Gaussian white noise [14]. A signal with correlated noise can be processed by a level-dependent wavelet shrinkage method [15].

A specific challenge in buckypaper nanomanufacturing is that the Raman spectra are usually provided with signal-dependent noise. In this paper, a generalized wavelet shrinkage method is proposed in order to make full use of the property of signal-dependent noise and to denoise the entire Raman spectrum of CNT buckypaper to enhance the signal of Raman spectra before feature extraction. Using this method, the data acquisition time can be reduced without compromising the S/N ratio. This method enables *in situ* quick quality control based on inline Raman spectroscopy and improves control accuracy, sensitivity, and efficiency. In addition, it can potentially improve the scalability of nanomanufacturing processes. To demonstrate the effectiveness of this method, we used a custom-made continuous Raman test setup and continuous buckypaper sample to conduct a case study. Both simulation and case study data have revealed that the proposed approach outperforms conventional wavelet denoising methods and improves the S/N ratio by up to 100%, which means only less than half of the original data acquisition time is required to obtain signals with an equivalent S/N ratio.

The remainder of this paper is organized as follows. Section II illustrates the noise source analysis for Raman

TABLE I
NOISE SOURCE AND PROPERTIES FOR DIFFERENT TYPES OF NOISE

Noise Types	Noise Sources	Characteristics
Photon Shot Noise	Statistical nature of light	Inescapable; Proportional to intensity
Sample-generated Noise	Sample composition ratio; Fluorescence	Temperature-dependent, heterogeneity-dependent (moving)
Instrument-Generated Noise	Detector noise such as thermal noise; variation in laser intensity	Temperature-dependent, provide useful information of performance of instrument
Computationally Generated Noise	Read out noise; converting electrons from the detector to a digital value	Independent with signal magnitude and measurement time
Externally Generated Noise	Fluorescent room lighting, sunlight, cosmic rays	Independent with signal magnitude

spectrum, as well as noisy signal modeling and validation. Section III describes a generalized wavelet shrinkage method developed in this paper and compares it with the conventional wavelet denoising method. Section IV presents a simulation study to validate the proposed wavelet shrinkage method. Section V demonstrates how the proposed method can be used in inline Raman characterization of buckypaper. Finally, a brief summary and future research possibilities are discussed in Section VI.

II. NOISE PATTERN ANALYSIS AND SIGNAL MODELING OF RAMAN SPECTRUM

A. Noise Source Analysis

In order to develop corresponding denoising and signal enhancement techniques for the Raman spectra of CNT buckypaper materials, noise sources and patterns should be analyzed first. Table I summarizes five types of noise in Raman spectra, including photon shot noise, sample-generated noise, instrument-generated noise, computationally generated noise, and externally generated noise [16].

Based on noise characteristics, we can propose a signal model of the Raman spectrum with the following facts or assumptions: 1) photon shot noise and sample-generated noise can be measured from noise in the Poisson process because the Raman scattering and photon arrival process follows a Poisson distribution and the influence of background counts is usually negligible [18]; 2) the readout noise is the main element of instrument-generated noise and computationally generated noise, which is assumed to be an additive Gaussian noise and is independent from the Poisson process; 3) the externally generated noise is negligible since specific measurements have been implemented to prevent effects of sunlight in the Raman instrument, which is verified by the fact that no spikes caused by cosmic rays were found in the training spectra; and 4) the temperature remains consistent during the short measurement time.

B. Signal Modeling of Raman Spectrum

A Raman instrument uses charge-coupled device cameras to identify the intensity of the scattered photons. The data collected by each frequency bin in a Raman instrument can be described by Snyder's model [17]

$$y_i = n_i^s + g_i \tag{1}$$

where y_i denotes data collected by the ith frequency bin in a Raman device, n_i^s is the number of photoelectrons generated on the ith bin ignoring the influence of background counts, g_i is the addictive Gaussian readout noise from the amplifier, and $n_i^s \sim \text{poisson}(\mu_i^s)$; $g_i \sim N(0, \varepsilon_g) \cdot n_i^s$ becomes larger as the acquisition time becomes longer. This can be observed in Fig. 1. n_i^s and g_i are assumed statistically independent. For Poisson distribution poisson(λ) with sufficiently large values of λ (e.g., $\lambda > 1000$), the Poisson distribution can be approximated by a normal distribution. Meanwhile, $\mu_i^s > 10^7$ is satisfied in the Raman spectroscopy analysis [18]. Thus, based on the normal approximation, $n_i^s \sim N(\mu_i^s, \mu_i^s)$, y_i follows a normal distribution with $N(\mu_i^s, \mu_i^s + \varepsilon_g)$.

The Raman spectra intensity is correlated with data collected by each frequency bin in the Raman device. Thus, (1) can be rewritten as

$$y(v) = s(v) + \sigma(s(v)) \cdot \varepsilon(v) \tag{2}$$

where $y(v)$ is the observed Raman intensity with respect to Raman shift v, $s(v)$ is the real Raman intensity, and $\sigma(s(v)) \cdot \varepsilon(v)$ is the signal-dependent noise with respect to Raman shift v in a Raman spectrum. $\sigma(\cdot)$ denotes the function of noise and Raman intensity and $\varepsilon(v)$ means Gaussian white noise under Raman shift v.

If we consider a linear relationship between the Raman intensity and the collected data in Raman detector [18], we can get that the $y(v)$ in (2) follows a normal distribution $N(s(v), a \cdot s(v) + b)$, and a and b can be obtained from historical data of the Raman spectra, which will be introduced in the next section.

The noise of Raman intensity under different Raman shifts is assumed to be uncorrelated, which is reasonable based on the validation test with real data shown in Section II-C. We can get the signal model of a Raman spectrum in a matrix form

$$\mathbf{Y} = \mathbf{S} + \mathbf{\Sigma} \sim N(\mathbf{S}, a \cdot \text{diag}(\mathbf{S}) + b \cdot \mathbf{I}) \tag{3}$$

where $\mathbf{Y}$ is the observed Raman intensity vector, which is column vector of $y(v)$ with respect to sequential Raman shift, $\mathbf{S}$ is the real Raman intensity vector whose items are $s(v)$ with sequential Raman shift, and Σ is the signal-dependent noise vector, which is the column vector of $\sigma(s(v)) \cdot \varepsilon(v)$ with respect to sequential Raman shift.

C. Validation of Raman Spectroscopy Modeling

Before the application of the Raman spectrum model, a detailed validation is required for two purposes: 1) to verify the model effectiveness, including the validity of the assumption and constitution used in the modeling efforts and 2) to obtain the key parameters from the experimental data. In this validation effort, eight groups of experiments

TABLE II
DESIGN OF EXPERIMENT FOR THE VALIDATION OF RAMAN SPECTRUM MODEL

Sample Type	Acquisition Time	Validated Parameter
SWCNT	0.05 second	$a=1$, $b=42$
SWCNT	0.1 second	$a=1$, $b=41$
SWCNT	0.5 second	$a=0.9$, $b=44$
SWCNT	1 second	$a=1$, $b=41$
MWCNT	0.5 second	$a=1$, $b=41$
MWCNT	1 second	$a=1$, $b=41$
MWCNT	2 second	$a=1$, $b=41$
MWCNT	5 seconds	$a=0.9$, $b=42$

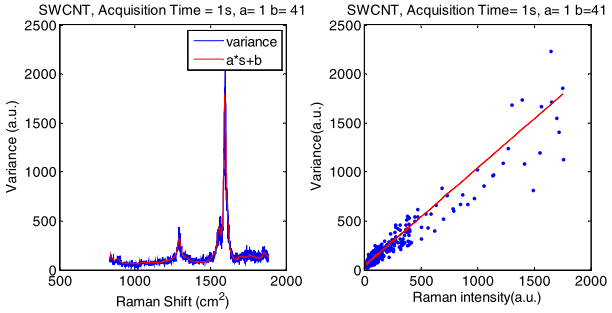

Fig. 2. (a) Comparison between variance and transformed Raman spectrum data. (b) Regression relationship between Raman shift and variance.

are designed and conducted with the parameters shown in Table II. The experiments used two types of samples: SWCNT buckypaper and multiwalled CNT (MWCNT) buckypaper. For the SWCNT buckypaper, each acquisition time setting (0.05, 0.1, 0.5, and 1 s) is replicated 50 times in order to obtain a relatively accurate estimation of the variance in every point of signal using a regular static Raman approach. Similarly, for the MWCNT buckypaper with different acquisition time settings (0.5, 1, 2, and 5 s) are replicated 50 times. Different acquisition time settings were used for the MWCNT and SWCNT buckypaper due to the different relationship between S/N ratios and acquisition time for the MWCNT and SWCNT. The details of the instrument and experiment process used in this validation are provided in Section V.

To validate the uncorrelated assumption of the noise under different Raman shifts, we repeated measuring 100 Raman spectra for the same sample. The average spectrum was also computed. After that, the correlation matrix among the Raman intensities under different Raman shifts is calculated. We can observe that the absolute value of the off-diagonal entries of the correlation matrix is consistently lower than 0.3. We then perform a hypothesis test with the null hypothesis that the noise is uncorrelated and the alternative hypothesis is that noise is correlated. The test result suggested that we cannot reject the null hypothesis at a significance level of 0.05.

To test the signal-dependent property of noise, the sample variance for every Raman shift can be calculated. In Fig. 2, we can see that the curved shape of the calculated variance at each point is very similar to the tuning of signals by a linear transformation. By calculating the Pearson product-moment correlation coefficient (PPMCC) [19], the PPMCC of variance vector and SWCNT signal is 0.958 and the PPMCC of variance vector and MWCNT signal is 0.901. Both of them are strongly correlated, which indicates that the noise is signal dependent and the noisy signal model can fit the signal and variance well. Fig. 2 shows the visual comparison between the variance and the transformed signal and regression relationship between Raman shift and variance for SWCNT with an acquisition time of 1 s. Moreover, based on the minimal mean square error principle, linear parameters a and b for every acquisition time setting of SWCNT and MWCNT have been validated. According to our validation results in Table II, the values of linear parameters a and b remain stable for different materials and different acquisition times, which indicates that the linear parameters are related only with Raman instrument itself, but are independent of the choice of materials and acquisition time. Validated linear parameters for different materials and acquisition time settings remain that $a = 1$ and $b = 41$.

In summary, the noise in Raman spectra, including photon shot noise, sample-generated noise, instrument-generated noise, computationally generated noise, and externally generated noise can be regarded as signal-dependent noise. And the dependence relationship remains stable and linear, that is, independent with different materials and acquisition time settings. Based on the training Raman spectra data from a buckypaper manufacturing process, the validated linear parameters are $a = 1$ and $b = 41$.

III. GENERALIZED WAVELET SHRINKAGE METHOD

To reduce data acquisition time without loss of the S/N ratio or the improvement of the S/N ratio within a fixed data acquisition time, a generalized wavelet shrinkage method is developed in this paper. The idea of generalized wavelet shrinkage is to make full use of the validated linear dependence between the signal and the noise and to promote the shrinkage from level dependent to adaptive individual dependent, that is to say, conventional wavelet shrinkage methods determine thresholds based on different levels of wavelet coefficients. For generalized wavelet shrinkage, the threshold is individually determined based on each wavelet coefficient. We will first discuss the discrete wavelet decomposition, in Section III-A, where Raman spectra are transformed into the wavelet domain. Then, a conventional wavelet shrinkage method will be introduced in Section III-B to implement wavelet coefficients shrinkage based on level-dependent thresholds. With the help of the validated signal noise dependence, the signal variance can be estimated and an individual threshold can be determined for each wavelet coefficient. These "customized" thresholds will adaptively cause shrinkage corresponding to the wavelet coefficients and achieve a higher S/N ratio. The detailed technique of the generalized wavelet shrinkage method and its relationship with the penalized optimization will be introduced in Section III-C. Section III-D implements the sensitivity analysis of diagonal approximation. Finally, Section III-E provides further discussion on the criteria for selection of the penalized parameter and wavelet basis.

A. Discrete Wavelet Decomposition

The wavelet transformation is selected to decompose Raman spectra because of the following characteristics: 1) wavelet-based modeling can handle complicated nonlinear Raman Spectra; 2) the wavelet-based method can analyze signals by multiresolution, which provides the opportunity for the diverse resolution analysis on different segments of Raman spectra; and 3) scarcity of wavelet coefficients is suitable for soft shrinkage and hard shrinkage, which are better than linear shrinkage, especially for nonstationary and nonlinear signals.

The first step should be transforming every Raman spectra into a wavelet domain. According to the wavelet theory [20], functions $\phi(\cdot)$ and $\psi(\cdot)$ are known as the scaling function (father wavelet) and wavelet function (mother wavelet), respectively. Usually, an orthonormal wavelet basis with basic properties is chosen. The standardized Raman spectrum data $g(v)$ are composed into two parts corresponding to coarse and detail parts. $g(v)$ belongs to the square-integral function space $L^2(\Re)$ [20]

$$g(v) = \sum_{k\in\mathbf{Z}} c_{sk}\phi_{sk}(v) + \sum_{j=s}^{\infty}\sum_{k\in\mathbf{Z}} d_{jk}\psi_{jk}(v)$$

where $\phi_{sk}(v)$ and $\psi_{jk}(v)$ are known as the scaling function and wavelet function. c_{sk} and d_{jk} are called the approximate coefficients and detail coefficients. They are determined by the inner product of $g(v)$ and a scaling function or a wavelet function.

According to the discrete wavelet transform algorithm, $g(v)$ can be divided into matrix product of wavelet coefficients and orthogonal wavelet basis. The matrix form of wavelet decomposition for noisy signal model (3) is

$$\mathbf{\Gamma}\cdot\mathbf{Y} = \mathbf{\Gamma}\cdot\mathbf{S} + \mathbf{\Gamma}\cdot\mathbf{\Sigma} \sim N(\mathbf{\Gamma}\cdot\mathbf{S}, a\cdot\mathbf{\Gamma}\cdot\mathrm{diag}(\mathbf{S})\cdot\mathbf{\Gamma}^T + b\cdot\mathbf{I}) \tag{4}$$

where $\mathbf{\Gamma}$ is the wavelet transform matrix that depends on the selected wavelet basis.

Equation (4) can be redefined as

$$\mathbf{W} = \mathbf{G} + \mathbf{E} \sim N(\mathbf{G}, \mathbf{\Lambda}) \tag{5}$$

where $\mathbf{W} = \mathbf{\Gamma}\cdot\mathbf{Y}$, $\mathbf{G} = \mathbf{\Gamma}\cdot\mathbf{S}$, and $\mathbf{\Lambda} = a\cdot\mathbf{\Gamma}\cdot\mathrm{diag}(\mathbf{S})\cdot\mathbf{\Gamma}^T + b\cdot\mathbf{I}$.

The scalar form of (5) is

$$w_i^J = g_i^J + e_i^J, \quad i = 1, \ldots, c^J$$

where w_i^J denotes the ith coefficients in wavelet decomposition level J transformed from observed signals, g_i^J denotes the ith coefficients' ingredients with respect to real signal in wavelet decomposition level J. e_i^J means the ith coefficients' ingredients with respect to signal-dependent noise in wavelet decomposition level J.

B. Wavelet Shrinkage Method

One of the most popular wavelet-based analysis methods is wavelet shrinkage for signal denoising and compression. This wavelet shrinkage method is asymptotically optimal for recovering objects taken from certain functional classes, such as the Besov spaces [21]. As for multivariate normal distribution, hard shrinkage and soft shrinkage are two widely used thresholding rules, which correspond to minimum complexity estimates for complexity penalties.

In order to fully understand the process, we first consider ℓ_2-norm penalty

$$\min_{\mathbf{W}}\{(\mathbf{Y} - \mathbf{\Gamma}^T\mathbf{W})^T(\mathbf{Y} - \mathbf{\Gamma}^T\mathbf{W}) + \lambda\mathbf{W}^T\mathbf{W}\} \tag{6}$$

where $\mathbf{\Gamma}$ is a wavelet transform matrix that depends on the selected wavelet basis, $\mathbf{Y}$ denotes the original signals' matrix, whose column means one Raman spectrum, $\mathbf{W}$ denotes the wavelet coefficients' matrix in the wavelet domain, and λ is a penalty parameter.

Because of the orthonormality of wavelet basis matrix, $\mathbf{\Gamma}^T\mathbf{\Gamma} = \mathbf{I}$, we can obtain the solution of (6) as

$$\hat{w}_i^J = \frac{1}{1+\lambda} w_i^J \tag{7}$$

where w_i^J denotes the original ith coefficients in wavelet decomposition level J transformed from the observed signals and $\hat{w}_i^J$ denotes the estimated (after denoised) ith coefficients in wavelet decomposition level J.

Straightforwardly, (6) has a quadratic penalty and corresponds to the linear shrinkage. Linear shrinkage cannot remove noise effectively in wavelet coefficients, so it can be difficult to find its usage in wavelet-based methods in the literature.

The soft shrinkage method is closely correlated with minimum complexity estimates with ℓ_1-norm penalty [21], which is similar to LASSO in regression [22]

$$\min_{\mathbf{W}}\{(\mathbf{Y} - \mathbf{\Gamma}^T\mathbf{W})^T(\mathbf{Y} - \mathbf{\Gamma}^T\mathbf{W}) + \lambda||\mathbf{W}||_{\ell_1}\}. \tag{8}$$

The soft shrinkage method can solve (8) with

$$\hat{w}_i^J = \eta_s\left(w_i^J, \frac{\lambda}{2}\right) = \mathrm{sign}(w_i^J)\left(|w_i^J| - \frac{\lambda}{2}\right)_+ \tag{9}$$

where $\eta_s(\cdot)$ denotes the soft shrinkage function, $\mathrm{sign}(\cdot)$ means the sign function, $(|w_i^J| - \lambda/2)_+ = (|w_i^J| - \lambda/2)I(|w_i^J| - \lambda/2)$, and $I(\cdot)$ is the indicator function. $\lambda/2$ is the threshold in the soft shrinkage function.

Similarly, hard shrinkage

$$\hat{w}_i^J = \eta_h\left(w_i^J, \sqrt{\lambda}\right) = \mathrm{sign}\left(w_i^J\right)\left(|w_i^J|\right)I\left(|w_i^J| - \sqrt{\lambda}\right) \tag{10}$$

is the solution to minimum complexity estimates with ℓ_0-norm penalty and here $\sqrt{\lambda}$ is the threshold [21]

$$\min_{\mathbf{W}}\{(\mathbf{Y} - \mathbf{\Gamma}^T\mathbf{W})^T(\mathbf{Y} - \mathbf{\Gamma}^T\mathbf{W}) + \lambda||\mathbf{W}||_{\ell_0}\}. \tag{11}$$

One explanation for the fact that a soft shrinkage function is preferred for smoothing is that it possesses various statistical advantages like continuity of the rule. While the hard shrinkage rule yields keep-or-kill estimation, it will protect larger values in the original signals, especially for peak values. In a buckypaper manufacturing process, D-band intensity peak and G-band intensity peak in a Raman spectrum are of great interest for monitoring and control. Therefore, the hard shrinkage method is preferred in our application.

The selection of threshold is one of the most important factors in the efficiency of wavelet denoising. Donoho and Johnstone [14] and Johnstone and Silverman [15] proposed three popular thresholding methods: VisuShrink,

RiskShrink, and SureShrink and compared them with minimax paradigm. The major difference among these three methods is the procedure to get the threshold. VisuShrink applies the universal threshold derived under the constraint that with high probability, the estimate should be at least as smooth as the signal; RiskShrink minimizes the theoretical upper bound of the asymptotic risk; and SureShrink minimizes the Stein unbiased estimate of risk for threshold estimates.

However, a common limitation of these conventional wavelet shrinkage methods is that the threshold can only be determined globally or level dependently. In another words, those methods use only the same threshold for all the wavelet coefficients in a given level. The variance of wavelet coefficients is estimated from the data directly. Thus, the intrinsic properties determine that the conventional wavelet shrinkage method cannot determine individual threshold for every wavelet coefficient. Instead, according to the discussion in Section II-C, we know that the noise of Raman spectra in buckypaper manufacturing processes has signal-dependent characteristics. Furthermore, the relationship of the signal-noise dependence remains stable and linear. Thus, we can estimate the noise based on a linear parameter from the validation process, which enables us to create a corresponding threshold for each individual wavelet coefficient. We will develop a current wavelet shrinkage method from a level-dependent thresholding to an individual-dependent thresholding, detailed in the next section.

C. Generalized Wavelet Shrinkage Method

A generalized wavelet shrinkage method is proposed to consider effects from the covariance matrix $a\cdot\mathbf{\Gamma}\cdot\text{diag}(\mathbf{S})\cdot\mathbf{\Gamma}^T+b\cdot\mathbf{I}$ multivariate Gaussian distribution in the wavelet-based analysis. However, there are two major differences between the generalized smoothing spline and the generalized wavelet shrinkage method.

1) The transformation basis matrix is different. One uses a wavelet basis, and the other a smoothing spline basis. In general, the coefficients in the wavelet domain are sparse, while coefficients in the spline domain are not sparse. Thus, a smoothing spline is suitable for fitting stationary smoothing signals, while wavelet analysis is more powerful for nonstationary and nonlinear noisy signals like Raman spectrum.
2) A generalized smoothing spline penalizes ℓ_2-norm, while a generalized wavelet shrinkage penalizes ℓ_1-norm or ℓ_0-norm. The reason for the different penalized order has been introduced in the previous section.

Considering the effect from covariance matrix $\mathbf{\Omega}=a\cdot\mathbf{\Gamma}\cdot\text{diag}(\mathbf{S})\cdot\mathbf{\Gamma}^T+b\cdot\mathbf{I}$, the wavelet-based minimum weighted sum of square estimate with ℓ_1-norm penalty is

$$\min_{\mathbf{W}}\{(\mathbf{Y}-\mathbf{\Gamma}^T\mathbf{W})^T\Omega^{-1}(\mathbf{Y}-\mathbf{\Gamma}^T\mathbf{W})+\lambda||\mathbf{W}||_{\ell_1}\}. \quad (12)$$

Based on Section III-B, we know that it should correspond to soft shrinkage. The solution of (12) can be obtained as

$$\min_{\mathbf{W}}\{(\mathbf{Y}-\mathbf{\Gamma}^T\mathbf{W})^T\mathbf{\Gamma}^T\mathbf{\Gamma}\mathbf{\Omega}^{-1}\mathbf{\Gamma}^T\mathbf{\Gamma}(\mathbf{Y}-\mathbf{\Gamma}^T\mathbf{W})+\lambda||\mathbf{W}||_{\ell_1}\}$$
$$\min_{\mathbf{W}}\{(\mathbf{\Gamma}\mathbf{Y}-\mathbf{W})^T\mathbf{\Gamma}\mathbf{\Omega}^{-1}\mathbf{\Gamma}^T(\mathbf{\Gamma}\mathbf{Y}-\mathbf{W})+\lambda||\mathbf{W}||_{\ell_1}\}$$

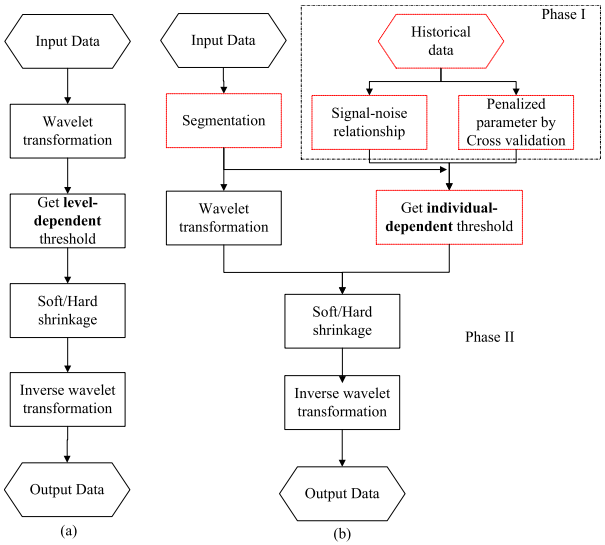

Fig. 3. Procedure for (a) conventional wavelet shrinkage and (b) generalized wavelet shrinkage. (Note: the main difference between a conventional wavelet shrinkage method and the generalized wavelet shrinkage method is highlighted by a red dotted frame.)

where $\mathbf{\Omega}$ is a diagonal positive definite matrix and Γ is an orthonormal wavelet basis set. Let $\mathbf{K}=\mathbf{\Gamma}\mathbf{\Omega}^{-1}\mathbf{\Gamma}^T$, since weak nondiagonal entries (most all of them are less than 10^{-4}, and maximum is 10^{-3}) are more than 15 times less than strong diagonal entries (the mean of diagonal entries is 0.015), $\mathbf{K}$ can be approximated with diagonal matrix with acceptable accuracy. In Section III-D, we will implement the sensitivity analysis of errors from the approximation by ignoring off-diagonal entries and describe the feasibility of the approximation.

The scalar solution of (12) is a generalized soft shrinkage

$$\hat{w}_i^J=\eta_s\left(w_i^J,\frac{\lambda}{2k_i^J}\right)=\text{sign}\left(w_i^J\right)\left(\left|w_i^J\right|-\frac{\lambda}{2k_i^J}\right)_+ \quad (13)$$

where k_i^J is a corresponding diagonal of matrix $\mathbf{K}=\mathbf{\Gamma}\mathbf{\Omega}^{-1}\mathbf{\Gamma}^T$ and $\lambda/2k_i^J$ is the threshold of soft shrinkage. $\lambda/2k_i^J$ is proportional to the standard deviation of w_i^J.

With the penalty of ℓ_0-norm, the minimal weighted sum of square estimate should solve the optimization of

$$\min_{\mathbf{W}}\{(\mathbf{Y}-\mathbf{\Gamma}^T\mathbf{W})^T\Omega^{-1}(\mathbf{Y}-\mathbf{\Gamma}^T\mathbf{W})+\lambda||\mathbf{W}||_{\ell_0}\}. \quad (14)$$

The generalized hard shrinkage is the solution

$$\hat{w}_i^J=\eta_h\left(w_i^J,\frac{\sqrt{\lambda}}{k_i^J}\right)=\text{sign}\left(w_i^J\right)\left(\left|w_i^J\right|\right)I\left(\left|w_i^J\right|-\frac{\sqrt{\lambda}}{k_i^J}\right). \quad (15)$$

Remarks:

1) The main idea of the generalized wavelet shrinkage method is to adaptively determine thresholds for shrinkage. Conventional wavelet shrinkage applies level-dependent thresholds to shrinkage wavelet coefficients since the variance cannot be estimated in every coefficient. The level-dependent threshold is suitable for a signal model with white noise. However, for signal-dependent noise in Raman spectra of buckypaper, the level-dependent threshold is not optimal because wavelet

coefficients within the same level share the same threshold, although they correspond to different noise amounts. Due to the stable and linear relationship between signal and noise variance, we can estimate the variance for every coefficient based on the validated signal model of Raman spectrum. Then, a generalized wavelet shrinkage method is designed to adjust the threshold individually for each coefficient, which outperforms the level-dependent threshold. It is notable that individual-dependent wavelet thresholds in generalized wavelet shrinkage do not mean that the thresholding parameters can be freely changing and individually adjusted. Different shrinkage thresholds for different wavelet coefficients are mainly caused by the noise level through the weighting matrix $\mathbf{\Gamma}\mathbf{\Omega}^{-1}\mathbf{\Gamma}^T$ and the shrinkage parameter λ, which is fixed through phase I analysis.

2) The procedure for conventional wavelet shrinkage method is shown in Fig. 3(a). The Raman spectra signals (input signals) are transformed into a wavelet domain first, and then level-dependent thresholds are estimated based on wavelet coefficients. Soft or hard shrinkage methods then adjust the values of wavelet coefficients, and the adjusted wavelet coefficients are inversely transformed into denoised Raman spectra signals (output signals). The procedure for the generalized wavelet shrinkage method can be separated into two phases, as shown in Fig. 3(b).
   a) During phase I, historical signals can be used to validate the signal model of Raman spectrum and get the parameters that indicate variance-signal relationship. Besides, a penalized parameter can be determined based on cross validation in phase I.
   b) For phase II, input signals can be divided into several segmentations according to different feature locations. For example, the D-band intensity peak and the G-band intensity peak are of interest in a continuous buckypaper manufacturing process, so these two segments can be specified. After the signal segmentation, a wavelet transformation is implemented to get wavelet coefficients. An individual wavelet threshold can be determined by the signal-noise relationship and penalized parameter from phase I and signals from phase II. The main difference between a conventional wavelet shrinkage method and the generalized wavelet shrinkage method is whether individual-dependent thresholding is implemented or not, which has been highlighted by the red dotted frames.
3) Assume that the noisy signals have no signal-dependent noise, the covariance matrix $\mathbf{\Omega}$ will be a scalar matrix (a scalar matrix is a diagonal matrix that has equal main diagonal entries). Then the thresholds for different wavelet coefficients $\lambda/2k_i^J$ will be the same. In this case, a generalized wavelet shrinkage will be equivalent to the wavelet shrinkage. Also, the stronger the signal-noise dependence property is, the better performance the generalized wavelet shrinkage has compared with the conventional wavelet shrinkage.
4) The generalized wavelet shrinkage method can also be used to build the calibration model or preprocess of the calibration spectroscopic samples. Usually, multivariate statistic techniques, such as principal component regression, partial least squares regression, or Gaussian process regression, are used to build the calibration model [22], [23]. However, these methods are with assumption that the spectroscopic data have Gaussian white noise. If wavelet coefficients are used as corresponding explanatory variables in a calibration model, generalized wavelet shrinkage approach can be used to build a calibration model for spectroscopic data with signal-dependent noise. Besides, if the corresponding explanatory variables in calibration are not wavelet coefficients, the generalized wavelet shrinkage can be applied to preprocess calibration spectroscopic samples with signal-dependent noise, which is able to prevent overfitting of calibration modeling and increase the model accuracy.

D. Sensitivity Analysis of Diagonal Approximation

In this section, we will implement the sensitivity analysis of errors from the approximation by ignoring off-diagonal entries and describe the feasibility of the approximation. Inspired by the diagonally dominant matrix, in which $|K_{ii}| > \sum_{j\neq i}|K_{ij}|$ for all i, we define $Q = (1/p)\sum_{i=1}^{p}(|K_{ii}|/\sum_{j\neq i}|K_{ij}|)$ to quantify the relative value of the diagonal entries compared with the summation of off-diagonal row entries. Q can also be regarded as the degree of diagonal dominance. For example, it is straightforward to show that for a diagonal dominant matrix, $Q \geqslant 1$. To perform the sensitivity analysis due to the approximation by ignoring off-diagonal entries under different Q. Similar to the simulation study, the spectra with signal-dependent noise is used for this sensitivity analysis. The generalized wavelet shrinkage with the diagonal approximation is used to denoise the original signal and obtain the estimated profile $\hat{y}_1$. Since the soft thresholding corresponds to the convex ℓ_1-norm penalty, we can also solve the original problem without diagonal approximation by applying convex optimization directly and obtain the estimated profile $\hat{y}_2$. We define the relative difference between $\hat{y}_1$ and $\hat{y}_2$ as $\text{DIFF} = \sum_{i=1}^{p}(|\hat{y}_{1i} - \hat{y}_{2i}|)/\sum_{i=1}^{p}(|\varepsilon_i|)$. The sensitivity relationship between DIFF and Q is shown in Fig. 4. From Fig. 4, we can conclude that the DIFF becomes smaller as the Q becomes larger, which is consistent with our intuition that the influence of diagonal approximation will be small if the diagonal entries are much larger than the off-diagonal entries. If the Q is smaller than 30, the DIFF quickly increases as the decrease in Q. In our application on Raman spectra, the Q is 77.61 (marked as a red star in Fig. 4), which results in about 10.6% difference of the accuracy corresponding to the noise standard deviation. The difference is about 1.02 units in Raman intensity, which is within the monitoring resolution based on the experience.

Though the diagonal assumption leads to some approximation errors (less than 1.02 units in this case), the proposed algorithm has significant computational advantages. The computation time of denoising one spectrum by our generalized

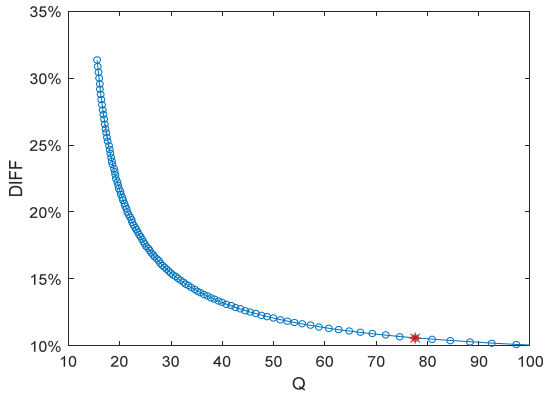

Fig. 4. Sensitivity analysis between DIFF and Q.

wavelet shrinkage (around 0.0009 s) is much faster than the computational time of using the convex optimization (around 1.0280 s). During the continuous manufacturing of the CNT buckypaper, multiple profiles will be measured and the computation time of using the convex optimization cannot satisfy the inline monitoring requirement, while the proposed generalized wavelet shrinkage can process the profiles efficiently and provide a very similar denoising result.

E. Criteria for Selection of the Penalized Parameter and the Wavelet Basis

1) Determine the Penalized Parameter by Revised Cross Validation: This section describes how to obtain the penalized parameter in phase I using in-control historical Raman spectra signals. Similar to the leave-one-out cross validation [24], the proposed approach balances the tradeoff between the bias and the variance of estimated parameters. The vital difference between the proposed approach and the regular leave-one-out cross validation is the choice of the benchmark vector in the optimization equation.

The proposed optimization equation is given as

$$\mathbf{W}_{n,\lambda}^{[k]} = \arg\min_{\mathbf{W}^{[k]}} (\mathbf{Y}^{[k]} - \mathbf{\Gamma}^T \mathbf{W}^{[k]})^T \mathbf{\Omega}^{-1} (\mathbf{Y}^{[k]} - \mathbf{\Gamma}^T \mathbf{W}^{[k]}) + \lambda ||\mathbf{W}^{[k]}||_{\ell_0} \quad (16)$$

where $k = 1, 2, \ldots, n$ and $\mathbf{Y}^{[k]}$ denotes the original signals' matrix except for the kth signal. $\mathbf{W}^{[k]}$ means corresponding wavelet coefficients' matrix without wavelet coefficients for the kth signal. $\mathbf{W}_{n,\lambda}^{[k]}$ represents the optimal wavelet coefficients' matrix under signal number n and penalized parameter λ. Optimal penalized parameter λ suffices minimum mean sum of square of difference between the estimated partial signals and ideal signals

$$\lambda^* = \arg\min_{\lambda \in \mathbb{R}^+} \frac{1}{n} \sum_{i=1}^{n} \left(\bar{\mathbf{Y}} - \mathbf{\Gamma}^T \mathbf{W}_{n,\lambda}^{[k]}(i)\right)^T \left(\bar{\mathbf{Y}} - \mathbf{\Gamma}^T \mathbf{W}_{n,\lambda}^{[k]}(i)\right) \quad (17)$$

where λ^* denotes the optimal penalized parameter. $\bar{\mathbf{Y}}$ represents the mean vector of all the Raman spectra by an ensemble average. Ensemble average will increase the S/N ratio based on the historical multiple measurements, so $\bar{\mathbf{Y}}$ can be regarded as the estimated ideal signals. $\mathbf{W}_{n,\lambda}^{[k]}(i)$ indicates the ith column of $\mathbf{W}_{n,\lambda}^{[k]}$, which represents wavelet coefficients' vector of the ith signal.

TABLE III
PERFORMANCE COMPARISON AMONG DIFFERENT WAVELET BASIS

Wavelet basis		λ	Mean $\lvert P_1 - P_1^* \rvert$	Std $\lvert P_1 - P_1^* \rvert$	Mean $\lvert P_2 - P_2^* \rvert$	Std $\lvert P_2 - P_2^* \rvert$
Raw Data	/	/	42.18	13.98	88.14	47.97
Coi	1	0.32	9.77	5.64	25.60	14.27
Coi	2	0.52	8.38	5.32	28.40	23.92
Coi	3	0.52	6.98	5.26	44.92	22.20
Coi	4	0.52	9.33	5.62	39.51	19.70
Coi	5	0.52	6.48	4.16	24.49	18.84
DB	4	0.32	10.31	7.15	37.94	34.97
DB	6	0.52	5.79	3.90	60.60	37.58
DB	8	0.36	7.88	6.35	41.94	27.39
DB	10	0.32	11.38	7.83	30.12	22.34
DB	12	0.52	16.35	5.20	31.50	21.25
DB	14	0.38	14.71	6.70	41.03	26.28
DB	16	0.34	12.42	7.28	24.34	20.59
DB	18	0.48	5.79	3.95	21.21	15.88
DB	20	0.50	7.58	5.43	59.69	19.56
Sym	4	0.52	12.90	5.46	34.04	26.66
Sym	5	0.36	9.49	8.12	27.17	25.99
Sym	6	0.52	12.78	5.55	33.50	24.58
Sym	7	0.34	8.93	8.02	25.92	20.32
Sym	8	0.52	14.93	5.49	25.90	20.71
Sym	9	0.50	6.40	4.08	29.33	27.72
Sym	10	0.52	6.00	4.78	24.71	16.26

* "DB" means "Daubechies wavelet", "Coi" denotes"Coiflet wavelet", 'Sym' denotes "Symmlet wavelet".

The vital difference between the proposed approach and the regular leave-one-out cross validation [24] is that applying $\bar{\mathbf{Y}}$ as an important benchmark vector in the optimization equation, instead of the kth signal in the regular leave-one-out cross validation. The reason for doing this is that an ensemble average $\bar{\mathbf{Y}}$ with high S/N ratio can be used to estimate ideal signals. Our target is picking up optimal penalized parameter that enables optimal denoising and signal enhancement instead of signal prediction.

2) Determine the Wavelet Basis: In practical applications, several factors should be considered when choosing the wavelet basis. They are orthogonality, complexity, width, and shape. Orthogonal wavelets produce wavelet spectra that contain discrete "blocks" of wavelet power and give the most compact representation of the signal. Complex wavelet function will return information about both amplitude and phase. Width will affect the resolution of the wavelet. In addition, the wavelet basis should reflect the types of features occurred in the signal [25]. According to the four factors above and the curve shape of Raman spectra, Coiflet, Daubechies, and Symmlet families are chosen and compared to analyze the Raman spectra.

Further wavelet basis selection is introduced as follows. As for each wavelet basis, optimal penalized parameter is obtained using the cross-validation method. The target of wavelet denoising and signal enhancement is to get the

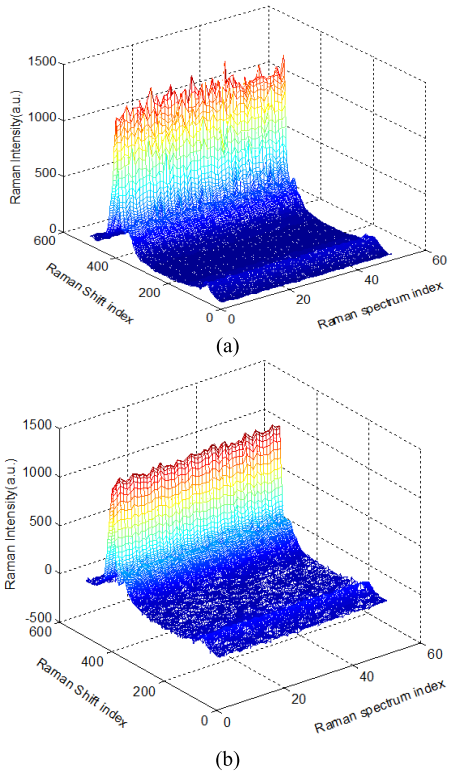

Fig. 5. Comparison between (a) wavelet shrinkage and (b) generalized wavelet shrinkage.

accurate D-band peak intensity and G-band peak intensity. Thus, the difference between every estimated optimal peak intensity (from ensemble average) and estimated denoising peak intensity is calculated during phase I, which is shown in Table III.

In Table III, P_1^* denotes the estimated optimal D-band peak intensity by ensemble average; P_1 is the estimated D-band peak intensity from denoised signals using optimal penalized parameter λ^*; and P_2^* and P_2 are the corresponding notations for G-band peak intensity. Four performance measures including mean of $|P_1-P_1^*|$, standard deviation of $|P_1-P_1^*|$, mean of $|P_2-P_2^*|$, and standard deviation of $|P_2-P_2^*|$ are considered totally to determine optimal wavelet basis as Daubechies 18.

IV. Simulation

We use the average of smoothing Raman spectra as the ideal signal. The D-band peak intensity value $P_1^* = 151.3$, and the G-band peak intensity value $P_2^* = 1231$. There are 50 Raman spectra generated by adding signal-dependent noise. In the simulation, conventional wavelet denoising is implemented using the procedures in Fig. 3(a), while the generalized wavelet shrinkage approach adopts the procedures in Fig. 3(b). Every signal is picked up as phase II signal in turn, and the remaining 49 Raman spectra are regarded as phase I historical data. The simulation results are summarized in the following discussions.

Fig. 5 shows a visual comparison between the denoised Raman spectra after wavelet shrinkage [Fig. 5(a)] and those with generalized wavelet shrinkage [Fig. 5(b)]. Obviously, the peak intensities of denoised signals after generalized wavelet shrinkage [Fig. 5(a)] are more uniform than peak intensities of denoised signals after wavelet shrinkage [Fig. 5(b)].

TABLE IV
Comparison Between Wavelet Shrinkage and Generalized Wavelet Shrinkage Based on Peak 1

	λ	Mean $\lvert P_1-P_1^*\rvert$	Std $\lvert P_1-P_1^*\rvert$	SNR
Raw data	/	44.34	17.90	1.21
WS	160	8.49	8.48	4.45
	170	8.42	8.48	4.47
	180	8.08	8.38	4.58
GWS	0.48	6.70	4.90	6.51
	0.58	6.70	4.90	6.51
	0.68	6.70	4.90	6.51

* WS means "Wavelet Shrinkage"; GWS means "Generalized Wavelet Shrinkage"

TABLE V
Comparison Between Wavelet Shrinkage and Generalized Wavelet Shrinkage Based on Peak 2

	λ	Mean $\lvert P_2-P_2^*\rvert$	Std $\lvert P_2-P_2^*\rvert$	SNR
Raw data	/	97.8082	52.7021	4.09
WS	260.00	47.79	35.35	7.40
	275.00	42.77	31.42	8.29
	290.00	40.04	28.28	9.00
GWS	0.14	24.77	19.11	14.02
	0.16	24.45	18.65	14.27
	0.18	25.12	18.87	13.98

Quantitatively, we can compare the SNR of Raman spectra after wavelet shrinkage and generalized wavelet shrinkage. As for peak 1, P_1^* denotes the estimated peak intensity that describes signal amplitude; $\text{mean}(|P_1 - P_1^*|) + \text{std}(|P_1 - P_1^*|)$ represents that bias and standard deviation from noise amplitude, and the calculation of SNR is

$$\text{SNR} = \frac{P_1^*/2}{\text{mean}\left(\left|P_1 - P_1^*\right|\right) + \text{std}\left(\left|P_1 - P_1^*\right|\right)}.$$

According to Table IV, we can see that for peak 1 intensity, the S/N ratio is equal to 1.21 without wavelet denoising. Applying wavelet shrinkage method will increase the S/N ratio from 1.21 to 4.47. Moreover, the generalized wavelet shrinkage approach we proposed will increase the S/N ratio from 1.21 to 6.51.

According to Table V, for peak 2, the S/N ratio can increase from 4.9 to 8.3 by wavelet shrinkage, and then to 14 by generalized wavelet shrinkage. Since the S/N ratio is correlated with the data acquisition time, the data acquisition time can be reduced without compromising the S/N ratio by this approach. This approach improves control accuracy, sensitivity, and efficiency, and potentially increases the scalability

Fig. 6. Renishaw inVia micro-Raman system with custom-designed remote optical probe and roller sample stage.

of nanomanufacturing processes. Besides, the lambda can be selected under an area, which means that the chosen penalized parameter is robust for the shrinkage.

V. Case Study: Investigation of Inline Raman Spectroscopy for Buckypaper Quality Monitoring

In this case study, we explored the feasibility of using an inline Raman spectroscopy on buckypaper samples to provide *in situ* data acquisition for quality control. The setup of inline Raman spectroscopy is shown in Fig. 6. SWCNT and MWCNT buckypaper samples were fabricated and measured with the Raman spectroscopy. The acquisition time for static Raman spectroscopy varies from 0.01 to 1 s for SWCNT buckypaper and from 0.1 to 5 s for MWCNT buckypaper. In all measurements, near infrared laser with a wavelength of 785 nm and a power of 150 mW was used to eliminate the effect of ambient light. Low-magnification lens was used to achieve larger focus tolerance.

For every acquisition time, we measured 50 Raman spectra and processed data by the wavelet shrinkage and generalized wavelet shrinkage discussed in Section III. The results for SWCNT buckypaper are given in Table VI. According to Table VI, with the acquisition time as 1 s, the S/N ratio for peak 1 can be increased from 5.41 to 8.97 by wavelet shrinkage and to 13.65 by generalized wavelet shrinkage, respectively. The increases in the S/N ratio are 65.86% and 152.34% for peak 1. For peak 2, the S/N ratio increases from 17.86 to 37 by wavelet shrinkage and to 39.68 by generalized wavelet shrinkage. Similar conclusions can be drawn that with different acquisition times, both wavelet shrinkage and generalized wavelet shrinkage can improve the S/N ratio, and generalized wavelet shrinkage improves more than conventional wavelet shrinkage. Also, the improvements of S/N ratios are different under different acquisition times. Based on the derivation of the generalized wavelet shrinkage, the performance of the generalized wavelet shrinkage will be similar to the conventional wavelet shrinkage if the noise has insignificant dependence on the strength of the signal. Usually, a longer acquisition time represents a higher intensity and stronger signal-noise dependence. In this situation, a generalized wavelet has a better performance than the conventional wavelet shrinkage.

TABLE VI
Comparison Between Wavelet Shrinkage and Generalized Wavelet Shrinkage With Raman Spectra on SWCNT Buckypaper

Exp time	/	Mean $\lvert P_1 - P_1^* \rvert$	Std $\lvert P_1 - P_1^* \rvert$	Mean $\lvert P_2 - P_2^* \rvert$	Std $\lvert P_2 - P_2^* \rvert$	Peak1 SNR	Peak2 SNR
T= 1	Raw data	15.58	10.31	29.76	19.42	5.41	17.86
	WS	8.21	7.4	14.99	8.73	8.97	37.04
	GWS	5.99	4.27	14.01	8.13	13.65	39.68
T= 0.5	Raw data	11.83	5.58	26.8	19.1	4.22	10.07
	WS	5.55	4.05	14.08	10.45	7.65	18.85
	GWS	5.04	3.77	12.06	7.27	8.33	23.92
T= 0.1	Raw data	12.63	5.63	13.45	10.2	1.11	5.46
	WS	4.39	2.47	8.38	7.47	2.94	8.15
	GWS	3.9	2.93	8.18	6.03	2.96	9.09
T= 0.05	Raw data	9.91	5.51	13.72	8.78	0.88	3.67
	WS	2.61	1.58	8.35	4.42	3.22	6.46
	GWS	2.53	1.58	6.44	4.01	3.28	7.89
T= 0.01	Raw data	10.67	3.66	13.2	8.95	0.59	2.30
	WS	2.42	2.02	6.36	4.85	1.91	4.55
	GWS	2.18	1.61	5.74	4.38	2.24	5.04

* WS means "Wavelet Shrinkage"; GWS means "Generalized Wavelet Shrinkage";

TABLE VII
Comparison Between Wavelet Shrinkage and Generalized Wavelet Shrinkage With Raman Spectra on MWCNT Buckypaper

Exp time	/	Mean $\lvert P_1 - P_1^* \rvert$	Std $\lvert P_1 - P_1^* \rvert$	Mean $\lvert P_2 - P_2^* \rvert$	Std $\lvert P_2 - P_2^* \rvert$	Peak1 SNR	Peak2 SNR
T= 5	Raw data	31.02	18.36	46.16	22.04	6.50	11.09
	WS	20.47	13.60	27.25	13.43	9.42	18.59
	GWS	16.17	12.04	24.58	6.63	11.37	24.23
T= 1	Raw data	15.67	7.36	19.15	10.63	2.86	5.26
	WS	4.44	2.67	6.96	5.22	9.26	12.85
	GWS	4.44	2.67	6.75	4.14	9.26	14.38
T= 0.5	Raw data	15.36	7.33	15.69	8.71	1.57	3.43
	WS	6.08	4.74	6.73	4.41	3.29	7.51
	GWS	3.93	2.38	6.85	3.64	5.65	7.97
T= 0.2	Raw data	10.95	4.37	12.88	6.90	1.12	1.97
	WS	4.40	4.60	5.19	4.26	1.91	4.12
	GWS	2.45	2.20	4.35	2.87	3.69	5.41
T= 0.1	Raw data	12.99	3.14	13.45	5.14	0.66	1.30
	WS	3.28	3.10	4.06	4.21	1.67	2.91
	GWS	1.96	2.05	3.38	2.66	2.67	3.99

The results for MWCNT buckypaper are shown in Table VII. With an acquisition time of 0.5 s for MWCNT buckypaper, the S/N ratio for peak 1 can rise from 1.57 to 3.29

by wavelet shrinkage and to 5.65 by generalized wavelet shrinkage, respectively. The increased percentage in the S/N ratio is 109.55% and 259.87% for peak 1. For peak 2, the S/N ratio increases from 3.43 to 7.51 by wavelet shrinkage and to 7.97 by generalized wavelet shrinkage.

According to the case study on SWCNT buckypaper and MWCNT buckypaper, the generalized wavelet shrinkage improves S/N ratio based on individual-dependent thresholding, which works better than the conventional wavelet shrinkage method. That means that the generalized wavelet shrinkage approach will improve the accuracy and efficiency of quality control of the CNTs buckypaper manufacturing process.

VI. Conclusion

Targeting the improvement of the S/N ratio and reducing data acquisition time for inline Raman spectroscopy, this paper focuses on developing a generalized wavelet shrinkage method to implement denoising of Raman spectrum that enables the use of Raman spectroscopy for inline monitoring and control for the nanomanufacturing process. Several vital contents and conclusions are summarized as follows.

The noise in Raman spectra, including photon shot noise, sample-generated noise, instrument-generated noise, computationally generated noise, and externally generated noise, are analyzed. The signal model of Raman spectrum is developed to describe the signal-noise dependence relationship. The model is validated by eight groups of experimental data with different types of CNTs buckypaper and different acquisition times. The results show that the value of linear parameters a and b remain stable and are not correlated with different materials and acquisition time. This allows for designing an adaptive denoising approach for individual wavelet coefficients.

Discrete wavelet decomposition can be implemented to transform Raman spectra signals into the wavelet domain. Based on the validated signal-noise dependence relationship, a novel generalized wavelet shrinkage approach is proposed to remove noise in every wavelet coefficient by individual adaptive wavelet thresholds, which outperforms the level-dependent conventional wavelet shrinkage method. The simulation and case study show the feasibility of the generalized wavelet shrinkage method. The technique can improve the S/N ratio dramatically or can be used to reduce data acquisition time without loss of S/N ratio, which lays a solid foundation for quick real-time monitoring and control of the nanomanufacturing process.

Moreover, the generalized wavelet shrinkage can be used to remove noise of signals with signal-dependent noise and realize better performance than the conventional wavelet shrinkage. Besides, it can also be applied to preprocess the calibration spectra with signal-dependent noise in order to prevent overfitting and improve the accuracy in calibration modeling.

In future research, a supervised control strategy will be investigated to adaptively adjust the scanning speed considering the signal-noise ratio of denoised spectra and the quantified quality features of buckypaper. Feature extractions need to be conducted after the denoising step for further process monitoring and control. Two types of control charts, control charts based on reconstructed signals and control charts based on wavelet coefficients, can be used to monitor different physical features. In addition, quality feature-based feedback control and automatic process control can be implemented to improve the quality of CNT buckypaper to scale-up nanomanufacturing processes.

Acknowledgment

The authors would like to thank the associate editor and the referees for constructive comments that substantially improved earlier drafts.

References

[1] H. H. Gommans, J. W. Alldredge, H. Tashiro, J. Park, J. Magnuson, and A. G. Rinzler, "Fibers of aligned single-walled carbon nanotubes: Polarized Raman spectroscopy," *J. Appl. Phys.*, vol. 88, no. 5, pp. 2509–2514, 2000.

[2] N. R. Raravikar, P. Keblinski, A. M. Rao, M. S. Dresselhaus, L. S. Schadler, and P. M. Ajayan, "Temperature dependence of radial breathing mode Raman frequency of single-walled carbon nanotubes," *Phys. Rev. B*, vol. 66, no. 23, p. 235424, 2002.

[3] T. Liu and S. Kumar, "Quantitative characterization of SWNT orientation by polarized Raman spectroscopy," *Chem. Phys. Lett.*, vol. 378, nos. 3–4, pp. 257–262, 2003.

[4] J. G. Park, S. Li, R. Liang, C. Zhang, and B. Wang, "Structural changes and Raman analysis of single-walled carbon nanotube buckypaper after high current density induced burning," *Carbon*, vol. 46, no. 9, pp. 1175–1183, 2008.

[5] G. Févotte, "*In situ* Raman spectroscopy for in-line control of pharmaceutical crystallization and solids elaboration processes: A review," *Chem. Eng. Res. Design*, vol. 85, no. 7, pp. 906–920, 2007.

[6] M. N. Alahbabi, Y. T. Cho, and T. P. Newson, "Long-range distributed temperature and strain optical fibre sensor based on the coherent detection of spontaneous Brillouin scattering with in-line Raman amplification," *Meas. Sci. Technol.*, vol. 17, no. 5, p. 1082, 2006.

[7] N. R. Abu-Absi *et al.*, "Real time monitoring of multiple parameters in mammalian cell culture bioreactors using an in-line Raman spectroscopy probe," *Biotechnol. Bioeng.*, vol. 108, no. 5, pp. 1215–1221, 2011.

[8] T. R. M. De Beer, W. R. G. Baeyens, J. Ouyang, C. Vervaet, and J. P. Remon, "Raman spectroscopy as a process analytical technology tool for the understanding and the quantitative in-line monitoring of the homogenization process of a pharmaceutical suspension," *Analyst*, vol. 131, no. 10, pp. 1137–1144, 2006.

[9] T. Ono, J. H. ter Horst, and P. J. Jansens, "Quantitative measurement of the polymorphic transformation of L-glutamic acid using *in-situ* Raman spectroscopy," *Crystal Growth Design*, vol. 4, no. 3, pp. 465–469, 2004.

[10] Q. Cheng, J. Bao, J. Park, Z. Liang, C. Zhang, and B. Wang, "High mechanical performance composite conductor: Multi-walled carbon nanotube sheet/bismaleimide nanocomposites," *Adv. Funct. Mater.*, vol. 19, no. 20, pp. 3219–3225, 2009.

[11] G. Wahba, *Spline Models for Observational Data*, vol. 59. Philadelphia, PA, USA: SIAM, 1990.

[12] P. M. Ramos and I. Ruisánchez, "Noise and background removal in Raman spectra of ancient pigments using wavelet transform," *J. Raman Spectrosc.*, vol. 36, no. 9, pp. 848–856, 2005.

[13] F. Ehrentreich, "Wavelet transform applications in analytical chemistry," *Anal. Bioanal. Chem.*, vol. 372, no. 1, pp. 115–121, 2002.

[14] D. L. Donoho and I. M. Johnstone, "Adapting to unknown smoothness via wavelet shrinkage," *J. Amer. Statist. Assoc.*, vol. 90, no. 432, pp. 1200–1224, 1995.

[15] I. M. Johnstone and B. W. Silverman, "Wavelet threshold estimators for data with correlated noise," *J. Roy. Statist. Soc., Ser. B (Statist. Methodol.)*, vol. 59, no. 2, pp. 319–351, 1997.

[16] M. J. Pelletier, "Quantitative analysis using Raman spectrometry," *Appl. Spectrosc.*, vol. 57, no. 1, pp. 20A–42A, 2003.

[17] D. L. Snyder, A. M. Hammoud, and R. L. White, "Image recovery from data acquired with a charge-coupled-device camera," *J. Opt. Soc. Amer. A*, vol. 10, no. 5, pp. 1014–1023, 1993.

[18] R. L. McCreery, *Raman Spectroscopy for Chemical Analysis*, vol. 225. New York, NY, USA: Wiley, 2005, pp. 37–41.

[19] M. Kutner, C. Nachtsheim, J. Neter, and W. Li, *Applied Linear Statistical Models*, 5th ed. Chicago, IL, USA: Irwin, 2005.
[20] I. Daubechies, *Ten Lectures on Wavelets*, vol. 61. Philadelphia, PA, USA: SIAM, 1992.
[21] E. J. Candés, "Modern statistical estimation via oracle inequalities," *Acta Numer.*, vol. 15, pp. 257–325, May 2006.
[22] T. Chen, J. Morris, and E. Martin, "Gaussian process regression for multivariate spectroscopic calibration," *Chemometrics Intell. Lab. Syst.*, vol. 87, no. 1, pp. 59–71, 2007.
[23] S. M. Clegg, E. Sklute, M. D. Dyar, J. E. Barefield, and R. C. Wiens, "Multivariate analysis of remote laser-induced breakdown spectroscopy spectra using partial least squares, principal component analysis, and related techniques," *Spectrochim. Acta B, At. Spectrosc.*, vol. 64, no. 1, pp. 79–88, 2009.
[24] M. H. Kutner, *Applied Linear Statistical Models*, vol. 4. Chicago, IL, USA: Irwin, 1996.
[25] C. Torrence and G. P. Compo, "A practical guide to wavelet analysis," *Bull. Amer. Meteorol. Soc.*, vol. 79, no. 1, pp. 61–78, 1998.

Xiaowei Yue (S'15) received the B.S. degree in mechanical engineering from the Beijing Institute of Technology, Beijing, China, in 2011, and the M.S. degree in power engineering and engineering thermophysics from Tsinghua University, Beijing, in 2013. He is currently pursuing the Ph.D. degree with the H. Milton Stewart School of Industrial and Systems Engineering, Georgia Institute of Technology, Atlanta, GA, USA.

His current research interests include *in situ* process control and variability reduction for nanomanufacturing.

Mr. Yue is a member of the American Society of Mechanical Engineers, the Institute for Operations Research and the Management Sciences (INFORMS), and the Institute of Industrial Engineers (IIE).

Kan Wang received the B.S. degree in theoretical and applied mechanics from Peking University, Beijing, China, in 2005, the M.S. degree in aircraft design from Beihang University, Beijing, in 2007, and the Ph.D. degree in industrial and manufacturing engineering from Florida State University, Tallahassee, FL, USA, in 2013.

He is currently a Post-Doctoral Fellow with the H. Milton Stewart School of Industrial and Systems Engineering and Georgia Tech Manufacturing Institute, Georgia Institute of Technology, Atlanta, GA, USA. His current research interests include nanomanufacturing, additive manufacturing, and printed electronics technologies and their applications in smart materials and biomedical devices.

Hao Yan received the B.S. degree in physics from Peking University, Beijing, China, in 2011. He is currently pursuing the Ph.D. degree with the H. Milton Stewart School of Industrial and Systems Engineering, Georgia Institute of Technology, Atlanta, GA, USA.

His current research interests include functional and high-dimensional data analysis and image-based process monitoring and diagnostics.

Mr. Yan is a member of the the Institute for Operations Research and the Management Sciences (INFORMS) and the Institute of Industrial Engineers (IIE).

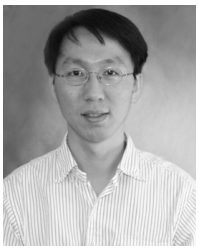

Jin Gyu Park received the B.S., M.S., and Ph.D. degrees in physics from Seoul National University, Seoul, South Korea, in 1997, 1999, and 2003, respectively.

He is currently a Research Faculty with the High-Performance Materials Institute, Florida State University, Tallahassee, FL, USA. His current research interests include the physical properties and characterization of carbon-related materials, including electrical/thermal transport, Raman spectroscopy of carbon materials, and electron microscopy of carbon nanotube and its composites.

Zhiyong Liang received the B.S., M.S., and Ph.D. degrees from the Beijing University of Aeronautics and Astronautics, Beijing, China, in 1987, 1990, and 2000, respectively, all in materials science and engineering.

He was an Associate Director of the Polymer and Composite Program at the Beijing University of Aeronautics and Astronautics. He is currently a Professor of Industrial and Manufacturing Engineering, Florida A&M University–Florida State University College of Engineering, Tallahassee, FL, USA, and the Director of the High-Performance Materials Institute, Florida State University, Tallahassee. His current research interests include carbon nanotube and its nanocomposite for multifunctional applications with enhanced structural and electrical/thermal properties, characterization of carbon nanotube/resin interface and packing structures, and scale-up nanomanufacturing.

Chuck Zhang received the B.S. and M.S. degrees in mechanical engineering from the Nanjing University of Aeronautics and Astronautics, Nanjing, China, in 1984 and 1987, respectively, and the Ph.D. degree in industrial engineering from the University of Iowa, Iowa City, IA, USA, in 1993.

He is currently a Professor with the H. Milton Stewart School of Industrial and Systems Engineering at the Georgia Institute of Technology, Atlanta, GA, USA. He has authored over 150 refereed journal articles and 180 conference papers. He holds 20 U.S. patents. His current research interests include additive manufacturing (3-D printing and printed electronics), advanced composite and nanocomposite materials manufacturing, and geometric tolerancing and metrology.

Ben Wang is the Chief Manufacturing Officer of the Georgia Institute of Technology, Atlanta, GA, USA, and the Executive Director of the Georgia Tech Manufacturing Institute, Atlanta. He is the Gwaltney Chair in Manufacturing Systems in the School of Industrial and Systems Engineering, Georgia Institute of Technology, where he is also a Professor in the School of Materials Science and Engineering. He has authored more than 200 papers in refereed journals and is a Co-Inventor of 25 patents or patent applications. With a primary research interest in applying emerging technologies to improve manufacturing competitiveness, he specializes in process development for affordable composite materials and is widely acknowledged as a pioneer in the growing field of nanomaterials. His current research interests include high performance and affordable composites, which is already changing product innovations worldwide.

Dr. Wang is a fellow of the Institute of Industrial Engineers, Society of Manufacturing Engineers, and Society for the Advancement of Materials and Process Engineering. He is a also a member of the National Materials and Manufacturing Board of the National Research Council.

Jianjun Shi received the B.S. and M.S. degrees in electrical engineering from the Beijing Institute of Technology, Beijing, China, in 1984 and 1987, respectively, and the Ph.D. degree in mechanical engineering from the University of Michigan, Ann Arbor, MI, USA, in 1992.

He is currently the Carolyn J. Stewart Chair Professor in the H. Milton Stewart School of Industrial and Systems Engineering and George W. Woodruff School of Mechanical Engineering, Georgia Institute of Technology, Atlanta, GA, USA. His current research interests include the fusion of advanced statistical and domain knowledge to develop methodologies for modeling, monitoring, diagnosis, and control for complex manufacturing systems.

Dr. Shi is a fellow of IIE, ASME, and INFORMS, an Academician of the International Academy for Quality, an Elected Member of the ISI, and a Life Member of ASA.